Component-level Biofidelity Assessment of Morphed Pedestrian Finite Element Models

David Poulard, Huipeng Chen, Jeff R. Crandall, Tomasz Dziewoński, Michal Pędzisz, Matthew B. Panzer

Abstract In pedestrian safety, human body models offer some promising advantages including the prediction of injury mechanisms, the interpretation of experimental results and a large potential of personalization. While model personalization via geometrical morphing allow accounting for anatomical differences, it is necessary to reassess each morphed model to ensure that morphing did not reduce the biofidelity of the model. In the present study, the AM50 THUMS pedestrian model (THUMS) was morphed to the anthropometric specifications of each of four cadavers (stature range: 1540–1820 mm; weight range: 46–114 kg) used in a series of vehicle–pedestrian impact tests. The baseline THUMS model and the four morphed THUMS models were evaluated using eleven component-level loading cases that were relevant for biomechanics of pedestrian impact, including some cases not evaluated previously with THUMS. The model responses were within the experimental corridors after scaling using mass and stature for the majority of the cases and subjects. The scaling approach was less effective for a model with extreme anthropometries (height: 1800 mm, weight: 55 kg) especially for cases involving local component tests.

Keywords kriging, scaling, model evaluation, mesh quality.

I. INTRODUCTION

Although significant improvements have been achieved in mitigating pedestrian fatalities, there are still over 400,000 pedestrians fatalities worldwide each year [1]. This suggests that an in-depth understanding of the complex interaction between the pedestrian and the vehicle is essential to ensure effective countermeasure designs.

Pedestrian finite element (FE) human body models (HBM) offer some promising advantages as advanced injury prediction tools in vehicle–pedestrian impact. The level of detail in thoracic and HBMs has increased due to the availability of detailed anatomical information and increased computing power [2]. Significant advances have also been made in material constitutive models, their implementation in finite element codes, and the required data used to define and validate them. One of the HBM used in vehicle–pedestrian impact is the Total Human Model for Safety (THUMS) pedestrian model [3], which has been widely used to investigate the biomechanics in vehicle–pedestrian impact [4-6].

The response of the human body to vehicle impact has been previously studied using post mortem human specimens (PMHS) [7-8]. These tests were the primary source of data for the development of the pedestrian HBM. From these studies, the biomechanical response of the pedestrian was greatly influenced by the pedestrian anthropometry and vehicle geometry. As PMHS differed in

D. Poulard is a Research Associate, H. Chen is a Ph.D. student, J. R. Crandall is a Professor and M.B. Panzer is an Assistant Professor at the University of Virginia Center for Applied Biomechanics in Charlottesville, VA, USA (tel: 434-296-7288x117, dp5fv@virginia.edu). T. Dziewoński is an Assistant Professor, M. Pędzisz is a Ph.D. student at Warsaw University of Technology in Warsaw, Poland.

anthropometries across subjects, it is believed that models with a generic anthropometry (e.g. 50th percentile male) cannot be properly evaluated against PMHS test data that differs from this idealized geometry.

While model personalization via morphing can reduce the geometric error of the computational model [9-12], each morphed model needs to be reassessed at the component-level to ensure that morphing did not reduce the biofidelity of the model. The goal of the current study is to evaluate the biofidelity of personalized pedestrian FE models at the component-level. In doing so, the effectiveness of scaling procedures commonly used to normalize biomechanical data will be investigated.

II. METHODS

Morphed pedestrian models

The AM50 THUMS pedestrian model (Academic version 4.0.1 for LS-Dyna) [3] was morphed to the anthropometric specifications of four PMHS (stature range: 1540–1820 mm; weight range: 46–114 kg, Table I) used in a series of vehicle–pedestrian impact tests [7]. The morphed pedestrian models varied greatly in stature and body shape relative to the baseline pedestrian model (Fig. 1).

TABLE I
GENERAL ANTHROPOMETRIC MEASUREMENTS

	1137-P	PMHS	1138-P	PMHS	1140-P	PMHS	1141-P	PMHS
Stature	1563	1540	1900	1830	1661	1610	1832	1820
Weight	65.9	72.6	119	114	84.4	86.2	55.2	46.3
BMI	27.0	30.6	33.0	34.0	30.6	33.3	16.4	14.0

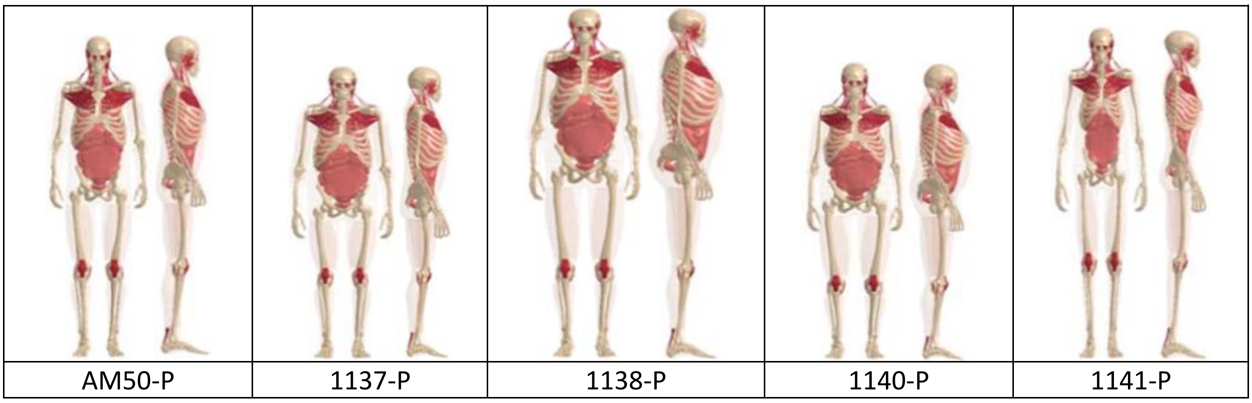

Fig. 1. Baseline and morphed pedestrian models.

The morphing procedure was based on a Dual Kriging interpolation [13] process using control points constructed from external anthropometric measurements (Table A in Appendix). This method has been used ability to generate personalized models from anthropometric landmarks by Pedzisz et al. (2012) [14], and it is a common technique used by other research groups in the computational biomechanics field [10-12]. This method alters only the shape of each HBM (and indirectly, the mass), while no change of the material properties was performed. All morphed models (labelled as 11XX-P) met mesh quality guidelines described in the THUMS manual, and were comparable to the baseline THUMS (AM50-P) model (Table II).

TABLE II
ELEMENT QUALITY REVIEW FOR THE MORPHED MODELS

Condition	Criteria	#elements violating criteria (%)				
		AM50-P	1137-P	1138-P	1140-P	1141-P
Timestep						
without mass scaling	1.00E-07	Yes	Yes	Yes	Yes	Yes
within a mass increase of 0.3%	4.00E-07	Yes	Yes	Yes	Yes	Yes
Element Size Max.	5 mm	73.8%	67.3%	87.9%	78.1%	60.7%
Element Size Min.	3 mm	13.4%	15.9%	7.1%	13.6%	20.8%
Warpage	< 50 deg	0.0%	0.0%	0.0%	0.0%	0.0%
Aspect Ratio	< 5.0	0.5%	0.0%	0.7%	0.5%	0.5%
Skew	< 60 deg	0.1%	0.1%	0.2%	0.1%	0.1%
Jacobian	< 0.3	0.0%	0.0%)	0.0%	0.0%	0.0%
Initial errors	-	None	None	None	None	None

Simulations

All five pedestrian models were validated using a series of component-level experiments described in this section (Table III). The experimental cases selected for evaluating the standing models were considered representative of the biomechanics of pedestrian impact, and included experimental cases not originally performed for the THUMS model. For body regions where experimental data was incomplete for validating the model, pedestrian dummy certification tests were used as a biofidelity target. Because some validation cases involved a subject in a seated posture, it was decided first that evaluation of the THUMS Occupant model (Academic version v4.01; AM50-O) would also be included for these cases to compare to the response of the pedestrian models.

All simulations were run using LS-Dyna v971 R6.1.1 (LSTC, Livermore, CA, USA). The pre- and post-processing analysis was carried out with LS-Prepost (v4.1, LSTC, Livermore, CA, USA) and scripts were written in Matlab (R2012a, The MathWorks Inc., Natick, MA, USA) for automated processing.

All model results were normalized to the 50th percentile male using the scaling procedures proposed by Mertz [16]. In this way, the response of all the HBM could be compared to experimental corridors that were not changed.

Head drop test

Isolated heads were dropped from a height of 14.8 inches on a steel plate in accordance with set out by NHTSA in 49CFR572.32 [17]. The peak resultant accelerations computed at the center of gravity of the head was normalized by the head mass (Table IV) and compared to the requirements (shall not be less than 225 g, and not more than 275 g).

Lateral shoulder impact

All models were evaluated in the shoulder lateral pendulum impact condition performed by Bendjellal et al. [18]. In these experiments, four subjects were seated on a hardwood horizontal surface with a vertical backrest. In the simulation, AM50-O was seated on a rigid plate and a pre-simulation was run to adjust the arm position of AM50-O to be consistent with the experiments (no posture change was required for the pedestrian models). A 23.4 kg impactor with a 4.3 m/s initial velocity was positioned laterally at the shoulder level, centered at the acromion (Fig. 2). The impact force was measured as the contact force between the impact and model. The force-time histories from the models were compared to the experimental corridors.

TABLE III
SIMULATION MATRIX

Region	Response	Reference	AM50-O	AM50-P 11XX-P
Head	Frontal Drop Test	49CFR572 [17]	No	Yes
Shoulder	Lateral Pendulum Test	Bendjellal et al (1984)[18]	Yes	Yes
Thorax	Frontal Pendulum Test	Kroell et al. (1971) [19]	Yes	Yes
Thorax	Lateral Pendulum Test	Shaw et al. (2006)[20]	Yes	Yes
Arm	Humerus three-point bending	Kemper and Duma (2005)[21]	No	Yes
Arm	Arm Lateral Compression	Kemper and Duma (2009)[22]	No	Yes
Abdomen	Anterior Bar Impact	Cavanaugh et al. (1986)[23]	Yes	Yes
Pelvis	Lateral Pendulum Test	Cesari et al (1982)[24]	Yes	Yes
Thigh	Femur three-point bending	Funk et al., 2004[25]	No	Yes
Knee	Knee Bending	Bose et al. (2008)[26]	No	Yes
Leg	Thigh three-point bending	Ivarsson et al. (2004)[27]	No	Yes

Thoracic frontal impact

All models were evaluated under thoracic frontal pendulum impacts performed by Kroell et al. [19]. In the simulation, AM50-O was seated on a rigid plate and a pre-simulation was run to adjust the initial position of the arm (no positioning required for the pedestrian models). An impactor with an initial velocity of 6.7 m/s was positioned at the mid-sternum level (Fig. 2). The impact force was measured as the contact force between the impact and model. Chest deflection was defined, using a method established in a previous study [28], as the variation of length between the middle of two nodes taken on the pectoral muscles and a node taken on the skin at T8 level (Fig. A in Appendix). The force-deflection curves from the FE models were compared to the experimental corridors redeveloped by Lebarbe and Petit [29]. Deflection was normalized to the chest depth of a 50th percentile subject (Table IV).

Thoracic lateral impacts

All models were evaluated in the lateral thoracic impact conditions from Shaw et al. [20]. In the simulation, AM50-O was seated on a rigid plate and a pre-simulation was performed on all models to reposition the arms. A 23.4 kg impactor with an initial velocity of 2.5 m/s was positioned under the axillary level, similar to the experiments (Fig. 2). The impact force was measured as the contact force between the impactor and model. The chest deflection was defined as the change in length between two bilateral nodes aligned with the center of the impactor (Fig. A) [28]. The force-deflection curves predicted by the models were compared to the experimental corridors normalized to the 50th percentile male developed by Shaw et al. [20]. Deflection was normalized to the chest breadth of a 50th percentile subject (Table IV).

Humerus three-point bending

Isolated humeri of the pedestrian models were evaluated in the three-point bending test conditions from Kemper et al. [21]. A 20 mm diameter spherical indentor was positioned at mid-shaft of the humerus and displaced into the bone at a rate of 3.0 m/s (Fig. 2). The indentor displacement and the contact force were compared to the experimental data.

Arm compression

Isolated upper arm of the pedestrian models were evaluated in the impact conditions of Kemper et al. [22]. A 14 kg, 152 mm diameter impactor with an impact velocity of 4 m/s was positioned above the center of the upper arm (Fig. 2). As in experiments [33], the upper arms were oriented vertically, with the medial side placed against a rigid wall. The impactor displacement was normalized to the arm diameter of a 50th percentile subject (Table IV) and both displacement and the rigid wall force were compared to the experimental corridors.

Anterior abdominal bar impact

All models were evaluated under abdominal anterior bar impact conditions performed by Cavanaugh et al. [23]. In the simulation, AM50-O was seated on a rigid plate and a pre-simulation was performed on all models to reposition the arms. A 33 kg, 25 mm diameter bar impactor with an initial velocity of 6.1 m/s was positioned at the L3 level (the average position in the experiment) (Fig. 2). The impact force was measured as the contact force between the impact and model. Abdominal penetration was defined as the variation of length between a node directly on the skin in contact with the bar and a node taken on the skin at L3 level (Fig. A). Penetration was normalized to the abdominal depth of a 50th percentile subject (Table IV).

Lateral pelvic pendulum impact

All models were evaluated under pelvic lateral pendulum impacts performed by Cesari et al. [24]. In the simulation, AM50-O was seated on a rigid plate while the pedestrian models were standing. A 17.3 kg spherical impactor with initial velocities of 5, 6, 7, 8, 9, 10 m/s was positioned laterally at the pelvic level, centered at the greater trochanter (Fig. 2). The impact force was measured as the contact force between the impact and the model. Force was normalized to the mass of the 50th percentile subject (Table IV). The normalized peak impact force-impact velocity from the FE models (occupant and pedestrian) were compared to the experimental corridors in ISO/TR 9790.

Femur three-point bending

Isolated femurs of the pedestrian models were evaluated in the three-point bending conditions by Funk et al. [25]. A 12 mm diameter cylindrical indentor, with loading rates of 1.2 m/s, was displaced into the mid-shaft of the femur up to failure (Fig. 2). Fracture in the femur model was determined using element elimination by setting the ultimate plastic strain to 1.6% [25]. The femoral deflection, contact force and the mid-shaft moment were outputted and compared to the experimental data.

Knee bending

Isolated knee joints of the pedestrian models were evaluated in valgus bending based on the test series by Bose et al. [26]. Bending rates were applied to the knee at a rate of 1.5 deg/ms, and ligament rupture was determined in post-processing by reviewing elements with plastic strain over 16% [5]. The knee moment-angle responses were outputted and compared to the experimental data [26]. The moment-angle history was geometrically scaled based on the theory of dimensional analysis [26] and compared to the experimental corridors.

Leg three-point bending

Intact legs of the pedestrian models were evaluated in latero-medial three-point bending based on the tests conducted by Ivarsson et al. [27]. The leg models were loaded to failure at a rate of 1.5 m/s. The tibial deflection, contact force and the mid-shaft moment were compared to the experimental data. Fracture in the tibia model was determined using element elimination by setting the ultimate plastic strain to 1.6% [25].

TABLE IV
ANTHROPOMETRIC MEASUREMENTS USED TO NORMALIZE DEFLECTIONS

	Experiments	**AM50-P**	**1137-P**	**1138-P**	**1140-P**	**1141-P**
Chest depth	214	247	249	221	331	261
Chest breadth	301	335	327	335	399	361
Arm diameter	78.5	100	109	130	110	62
Abdominal depth	288	264	235	356	313	166

III. RESULTS

The time series of each of the eleven validation cases of the AM50-P model is shown in Fig. 2. These responses were also typical of the responses with the morphed models. Scaled output from all simulated cases is presented in Fig. 3, along with experimental corridors associated with each case. Table V contains the peak values for all outputs measured for each morphed model in the current study including the average value obtained in the experiments (if available).

The average value of the peak scaled resultant head accelerations from the head drop impact simulation [17] was 196 ± 49.3 g, and none of the scaled model responses were within the 225–275 g certification requirements [17] except for AM50-P model which was already 50th percentile male geometry (268 g).

The average value of peak scaled force output in the shoulder impact was 2.3 ± 0.2 kN for the models, and the force predicted by the models closely agreed with the experiments corridors [18] (Fig, 3b). All models were within the corridors for the duration of the simulation, except during the loading phase of the lightest model (1141-P). The overall kinematic response differs between occupant model and pedestrian models as AM50-O exhibits slightly higher shoulder lateral excursion than the pedestrian models (131 mm vs. 109 ± 14 mm). This was likely due to the difference in arm posture between the occupant and the pedestrian models.

The model responses for the frontal thoracic impact [19] are presented along with the experimental corridors in Fig. 2c. The average value of the peak scaled force for the models was 4.0 ± 0.2 kN, and compared well to the experimental average peak force of 4.3 kN. The overall kinematic response differed between AM50-O and AM50-P as the occupant model exhibits lower sternal excursion than the pedestrian (154 mm vs. 175 mm). All model force–deflection responses were close to the lower bound of the corridors for most of the simulation, except during a portion of the loading phase.

In the thoracic lateral impact, the average scaled peak force was 1.3 ± 0.1 kN for the models, which was comparable to the average peak force measured in the experiments (1.4 ± 0.2 kN) [20]. However, the model outputs were out the corridor during the loading phase, up to 8% of deflection. Additional simulations with different impactor positions (± 20 mm along the vertical and horizontal axis) and arm postures (± 5°) were run using AM50-O to investigate where impactor position was responsible for this discrepancy, but the results were not sensitive to these changes. The deformation energy computed from the responses of AM50-O and AM50-P (25 J) were noticeably lower than the deformation energy suggested by the experimental corridors (33 ± 5 J). Because the initial energy condition was constant for all cases (72 J), a higher portion of energy was transferred to the models as kinetic energy than the PMHS.

The average scaled peak force in the abdominal impact simulations was 4.6 ± 0.7 kN, while the peak of the experimental average was 4.0 kN [23]. The seated AM50-O model exhibited lower abdominal excursion than the standing pedestrian models (171 mm vs. 227 ± 19 mm). The model outputs were within the corridors throughout most of the deflection, except for the heaviest model (1138-P). All models because noticeably stiffer than the experimental response beyond 30% deflection. The increase in stiffness observed in was due to the extreme compression of the solid elements of the organs (>90%), suggesting that the impactor was almost in contact with the lumbar vertebra at this time.

The average scaled peak forces in the pelvis impact simulations were 3.6 ± 0.3 kN at 5 m/s, 4.6 ± 0.4 kN at 6 m/s, 5.5 ± 0.5 kN at 7 m/s, 6.6 ± 0.5 kN at 8 m/s, 7.8 ± 0.7 kN at 9 m/s and 8.9 ± 1.0 kN at 10 m/s. These values were within the experimental corridors developed in ISO/TR 9790 (Fig. 3).

The average scaled model failure force and displacement in the humerus three-point bending case were 8.7 ± 2.8 kN and 12.5 ± 1.5 mm, while it was 4.3 ± 0.6 kN and 9.5 ± 1.2 mm in the experiments (n=3). All scaled model outputs were outside of the experimental corridors, except for the lightest model (1141-P). The average scaled model stiffness at 5 mm of displacement was 1.0 ± 0.3 kN/mm, approximately twice that of the average experimental stiffness (0.6 ± 0.1 kN/mm).

The average scaled peak force in the arm compression simulations was 9.5 ± 1.4 kN, and was comparable to the average experimental results (10.0 ± 3.3 kN). All models were within the corridors for the duration of the simulation except for the heaviest model (1138-P), which was stiffer than the PMHS data. Failure was not observed in the simulations, which was consistent with the experiments.

The average scaled model failure force and moment in the femur three-point bending simulations were 4.6 ± 1.6 kN and 517.4 ± 185 Nm respectively, and was comparable to the 4.3 ± 0.7 kN and 458 ± 95 Nm responses measured in the experiments. Variability in model failure force and moment was dominated by the results obtained by the lightest model (1141-P), which were substantially lower (1.9 kN and 216 Nm).

In lateral knee bending, the average model ligament rupture occurred at a bending angle of 18.2 ± 2.4° and a scaled moment of 250 ± 42.0 Nm, while the experimental data reported a bending angle of 14.1 ± 1.7° and a moment of 112 ± 29 Nm. The knee moment angle responses of the models were above the experimental data for all models, except for the lightest model (1141-P) which was less stiff than the other models and within the experimental corridors.

Finally, the average scaled model failure force in the leg three-point bending cases was 2.9 ± 1.0 kN, which was similar to the average failure force reported in the corresponding experimental study (2.9 ± 0.2 kN). Variability in model failure force was primarily due to the results of the lightest model (1141-P), which had a scaled failure force considerably lower than the other responses (1.3 kN).

IV. DISCUSSION

This study focused on evaluating four morphed pedestrian FE models of vastly different anthropometries at the component-level. The intended use of these models will be for a follow-on study investigating the biomechanics of vehicle–pedestrian impacts. The model geometry was morphed using anthropometric data extracted from four PMHS used in published pedestrian impact tests. While the morphing process substantially affected the component-level response of the pedestrian models, the normalized model responses were generally within the experimental responses and corridors for the majority of the eleven cases evaluated. Cases where the models did not agree with the PMHS results included the thoracic lateral impact, frontal head impact, and knee bending. In the thoracic lateral impact test, the morphed models were more compliant than experiment. These results suggest the model will likely overestimate the compression of the internal organs during a collision with a mid-size vehicle [5]. Additionally, one particular model (1141-P), which was an extremely underweight subject (height: 1800 mm, weight: 55 kg), produced biomechanical responses inconsistent with the other models. The cases where this particular model was an outlier were the pelvic impact and all three-point bending (humerus, femur, knee, leg).

The morphing method used in this study did not significantly change mesh quality, although morphing can potentially affect the model robustness by creating distorted elements. In this study, the morphed models were robust in all simulated cases without numerical instability. We attribute robustness and good element quality to the approach of morphing the whole body in one step rather than morphing individual segments in increments. Nevertheless, the morphing process was not able to exactly match every target in the mesh guideline since the baseline mesh topology was kept consistent for all the models. This was particularly evident for one model (1141-P) that was already highlighted previously as having an extreme anthropometry. While it was shown that the location of the control points influences the final shape and capabilities of target models [9-10], no extensive sensitivity study on the location of control points used for morphing was performed in the present study. The main focus was on stability and overall fit to the anthropometric data.

In all cases, outputs were scaled to a 50th percentile using Mertz method [15] to facilitate comparison with experiments across models. While minimal shifts to the response curves resulted from normalizing the baseline pedestrian model responses (only a 1 kg adjustment), significant differences in scaling factors were observed for the morphed models (weight range of 55 kg to 117 kg). In general, the Mertz scaling procedure was effective for the cases involving full body as the scaled responses were similar (Fig. 2(a) and (b)). This was a notable result given that this scaling method does not consider the non-linear and viscoelastic material responses that would be involved in defining the biomechanical response of the models. Where the simplified scaling method was less successful was in normalizing for local component tests (Fig. 2(c)) as it does not account for the differences in the local variation of limb mass to total body mass or body thickness. Consequently, developing new tools for scaling between different anthropometries is an active area of research [30].

In addition to Mertz scaling approach [15], deflection was normalized by a representative length corresponding to the loading path. The representative lengths of the model often differed significantly from the average lengths of the PMHS as the morphed models present a variety anthropometry. Normalizing deflection is equivalent to scaling response for stiffness. While this approach was appropriate for thoracic impact where the whole rib cage is involved, it might not be appropriate for some cases involving substantial localized deformation of soft tissues. For instance in the abdominal bar impact test, the abdomen tissue is relatively soft and the early force response was mainly influenced by local mass recruitment of the flesh and not the stiffness of the abdomen [30]. Consequently, scaling using the depth of soft tissues in front of the spine instead of using an overall abdominal depth could be more efficient in abdominal bar impact.

Human body models offer some promising advantages including the prediction of injury mechanisms, the interpretation of experimental results and a large potential of personalization. While model personalization via geometrical morphing was the focus of the study, with material properties assumed invariant, any sort “personalization” would also include modifications to material properties to account for age/gender.

V. CONCLUSION

The baseline THUMS model and the four morphed THUMS models were evaluated using eleven component-level loading cases that were relevant for biomechanics of pedestrian impact, including some cases not evaluated previously with THUMS. The model responses were within the 50^{th} percentile experimental corridors after normalizing the responses to the 50^{th} percentile male using Mertz scaling procedures for most of the whole body cases and subjects. However, the simplified scaling approach was less effective for cases involving component-level tests and models with extreme anthropometries. Therefore, caution should be used when using simplified normalization procedures for biomechanical data during corridor development or model evaluation.

VI. ACKNOWLEDGEMENTS

This work was supported by Toyota Collaborative Safety Research Center. The authors would like to acknowledge Aaron Steinhilb and Robert Paneck (Toyota Motor Engineering & Manufacturing, North America) for their contribution to the design of the study. Note that the views expressed in this paper are those of the authors and do not necessarily represent or reflect the views of the sponsors.

VII. REFERENCES

[1] Naci, H., Chisholm, D. and Baker, T. D. Distribution of road traffic deaths by road user group: a global comparison. *Injury prevention*, 2009, 15(1):55–9.

[2] Yang, K. H., Hu, J., White, N. A., King, A. I., Chou, C. C. and Prasad, P. Development of numerical models for injury biomechanics research: a review of 50 years of publications in the Stapp Car Crash Conference. *Stapp Car Crash Journal*, 2006, 50:429–90.

[3]. Maeno, T. and Hasegawa, J. Development of a finite element model of the total human model for safety (THUMS) and application to car-pedestrian impacts. *Proceedings of 17th international ESV Conference*, 2001, Amsterdam (Netherlands).

[4] Han, Y., Yang, J., Mizuno, K. and Matsui, Y. Effects of vehicle impact velocity, vehicle front-end shapes on pedestrian injury risk. *Traffic Injury Prevention*, 2012, 13(5):507–18.

[5] Watanabe, R., Katsuhara, T., Miyazaki, H., Kitagawa, Y. and Yasuki, T. Research of the relationship of pedestrian injury to collision speed, car-type, impact location and pedestrian sizes using human FE model (THUMS Version 4). *Stapp Car Crash Journal*, 2012, 56:269–321.

[6] Paas, R., Davidsson, J., Masson, C., Sander, U., Brolin, K. and Yang, J. Pedestrian shoulder and spine kinematics in full-scale PMHS tests for human body model evaluation. *Proceedings of IRCOBI Conference*, 2012, Dublin (Ireland).

[7] Subit, D., Kerrigan, J., et al. Pedestrian-vehicle interaction: kinematics and injury analysis of four full scale tests. *Proceedings of IRCOBI Conference*, 2008, Bern (Switzerland).

[8] Kerrigan, J., Crandall, J. R. and Deng, B. Pedestrian kinematic response to mid-sized vehicle impact. *International Journal of Vehicle Safety*, 2007, 2(3):221–240.

[9] Besnault, B., Guillemot, H., Robin, S., Lavaste, F. and Le Coz, J. Y. Morphometric study of the human pelvis. *Journal of Biomechanics*, 1998, 31(1):9–19.

[10] Poulard, D., Bermond, F., Dumas, R., Bruyere, K. and Compigne, S. Geometrical personalisation of human FE model using palpable markers on volunteers. *Computer Methods in Biomechanics and Biomedical Engineering*, 2012, 15:298–300.

[11] Bertrand, S., Skalli, W., Delacherie, L., Bonneau, D., Kalifa, G. and Mitton, D. External and internal geometry of European adults. *Ergonomics*, 2006, 49(15):1547–64.

[12] Serre, T., Brunet, C., et al. HUMOS (Human Model for Safety) Geometry: From One Specimen to the 5 th and 95 th Percentile. *Proceedings of the Digital Human Modeling for Design and Engineering Conference*, 2006, Lyon (France).

[13] Trochu, F. A contouring program based on dual kriging interpolation. *Engineering with computers*, 1993, 9(3):160–77.

[14] Pędzisz, M. and Dziewoński, T. Development of 5th and 95th scaled occupant thorax model. Influence of reference anthropometry data and kriging parameters on rib-cage shape and FE model dynamic response. *Proceedings of the International Crashworthiness Conference*, 2012, Milano (Italy).

[15] Toyota Motor Corporation. THUMS_AM50_V4AC Manual.

[16] Mertz, H. J. A procedure for normalizing impact response data. Society of Automotive Engineers, 1984, 840884, Warrendale, PA.
[17] ISO. Head Impact Protection: Final Rule, 49 CFR. Parts. 571(572): pp. 92–98.
[18] Bendjellal, F., Walfisch, G., Fayon, A. and Tarriere, C. A.P.R. Biomechanical Data. Nanterre, France, 1984.
[19] Kroell, C., Schneider, D. and Nahum, A. Impact tolerance and response of the human thorax, in biomechanics of impact injury and injury tolerances of the thorax-shoulder complex. *Proceedings of the 15th Stapp Crash Conference*, 1971 (710851).
[20] Shaw, J. M., Herriott, R., McFadden, J., Donnelly, B. and Bolte, J. Oblique and lateral impact response of the PMHS thorax. *Stapp Car Crash Journal*, 2006, 50:147–67.
[21] Kemper, A., Stitzel, J., Duma, S., Matsuoka, F. and Masuda, M. Biofidelity of the SID-IIs and a modified SID-IIs upper extremity: biomechanical properties of the human humerus. *Proceedings of 19th international ESV Conference*, 2005, Washington D.C. (USA).
[22] Kemper, A. and Duma, S. Development of Response Corridors for the Compressive Stiffness of the Male and Female Arm in Lateral Loading. *Proceedings of 21st international ESV Conference*, 2009, Stuttgart (Germany).
[23] Cavanaugh, J. M., Nyquist, G., Goldberg, S. and King, A. Lower abdominal tolerance and response. *Proceedings of the 30th Stapp Car Crash Conference*, 1986, San Diego (USA).
[24] Cesari, D., Ramet, M. and Clair, P-Y. Evaluation of pelvic fracture tolerance in side impact. *Proceedings of the 24th Stapp Car Crash Conference*, 1980, Michigan (USA).
[25] Funk, J. R., Kerrigan, J. R. and Crandall, J. R. Dynamic bending tolerance and elastic-plastic material properties of the human femur. *Proceedings of the Annual Association for the Advancement of Automotive Medicine Conference*, 2004, 48:215–33.
[26] Bose, D., Bhalla, K. S., Untaroiu, C. D., Ivarsson, B. J., Crandall, J. R. and Hurwitz, S. Injury tolerance and moment response of the knee joint to combined valgus bending and shear loading. *Journal of Biomechanical Engineering*, 2008, 130(3):031008.
[27] Ivarsson, J., Lesley, D., et al. Dynamic response corridors and injury thresholds of the pedestrian lower extremities. *Proceedings of the IRCOBI Conference*, 2004, Graz (Austria).
[28]Poulard, D., Kent, R. W., Kindig, M., Li, Z. and Subit, D. Thoracic response targets for a computational model: a hierarchical approach to assess the biofidelity of a 50th-percentile occupant male finite element model. *Journal of the Mechanical Behavior of Biomedical Materials*, 2015, 45:45–64.
[29] Lebarbé, M. and Petit, P. New biofidelity targets for the thorax of a 50th percentile adult male in frontal impact. *Proceedings of the IRCOBI Conference*, 2012, Dublin (Ireland).
[30] Nie, B., Kim, T., Crandall, J., Wang, Y. and Bollapragada, V. A Structure-based Scaling Approach for the Development of Pediatric Multi-Body Human Model. *Proceedings of the ICRASH Conference*, 2014, Sarawak (Malaysia).
[31] Beillas, P. and Berthet, F. Performance of a 50th percentile abdominal model for impact: effect of size and mass. *European Society of Biomechanics Conference*, 2012, Lisbon (Portugal).

TABLE V

NORMALIZED PEAK PARAMETER FOR EACH CASE FOR THE MODELS COMPARED TO EXPERIMENTS

Case	Models								Experiments	
Peak parameter [unit]	**AM50-O**	**AM50-P**	**1137-P**	**1138-P**	**1140-P**	**1141-P**	**Average (n=6)**	**S.D. (n=6)**	**Average**	**S.D.**
Head Drop Impact										
Peak acceleration [g]	-	268.8	212.6	202.3	149.7	151.6	197.0	49.3	N/A	
Shoulder Impact										
Peak force [kN]	2.35	2.21	2.02	2.32	2.34	2.29	2.26	0.13	N/A	
Thoracic Frontal Impact										
Peak force [kN]	4.03	4.01	4.11	3.72	4.26	3.67	3.97	0.23	4.30	0.89
Peak deflection [%]	31.4%	29.6%	29.4%	30.7%	31.9%	29.5%	30.4%	1.1%	38.9%	1.9%
Thoracic Lateral Impact										
Peak force [kN]	1.21	1.37	1.31	1.32	1.18	1.26	1.27	0.07	1.41	0.18
Peak deflection [%]	12.7%	12.5%	12.5%	13.1%	14.0%	13.9%	13.1%	0.7%	12.0%	3.8%
Humerus Three-point Bending										
Peak force [kN]	-	8.78	9.80	11.84	9.32	4.22	8.79	2.80	4.31	0.56
Arm Compression										
Peak force [kN]	-	9.90	8.18	7.85	10.36	11.05	9.47	1.39	10.04	3.36
Peak deflection [%]	-	57.1%	48.5%	40.3%	48.9%	55.8%	50.1%	6.7%	62.3	11.8
Abdominal Impact										
Peak force [kN]	*4.70*	3.82	4.75	5.42	5.31	3.69	4.62	0.73	3.1	0.95
Peak deflection [%]	*42.1%*	43.0%	39.7%	39.0%	40.0%	40.0%	40.6%	1.5%	55.3%	8.1%
Pelvic Impact										
5 m/s - Peak force [kN]	3.74	3.67	3.43	4.18	3.64	3.20	3.64	0.33	5.33	0.93
6 m/s - Peak force [kN]	4.65	4.55	4.35	5.15	4.63	3.99	4.55	0.38	6.24	1.09
7 m/s - Peak force [kN]	5.45	5.50	5.24	6.21	5.58	4.79	5.46	0.46	7.14	1.26
8 m/s - Peak force [kN]	6.49	6.47	6.63	7.21	6.89	5.76	6.58	0.49	8.06	1.43
9 m/s - Peak force [kN]	7.40	7.70	7.83	8.76	8.20	6.62	7.75	0.73	8.97	1.59
10 m/s - Peak force [kN]	8.21	9.10	8.88	10.30	9.67	7.46	8.94	1.01	9.87	1.74
Femur Three-point Bending										
Peak force [kN]	-	4.76	4.88	5.18	6.53	1.93	4.65	1.68	4.35	0.75
Peak deflection [mm]	-	18.4	17.3	19.4	20.1	11.7	17.4	3.3	17.6	3.8
Knee three-point bending										
Peak moment [Nm]	-	247.3	274.6	281.1	268.9	178.5	250.1	42.0	112.0	29.0
Leg three-point bending										
Peak force [kN]	-	3.87	2.75	3.08	3.56	1.29	2.91	1.0	2.90	0.22

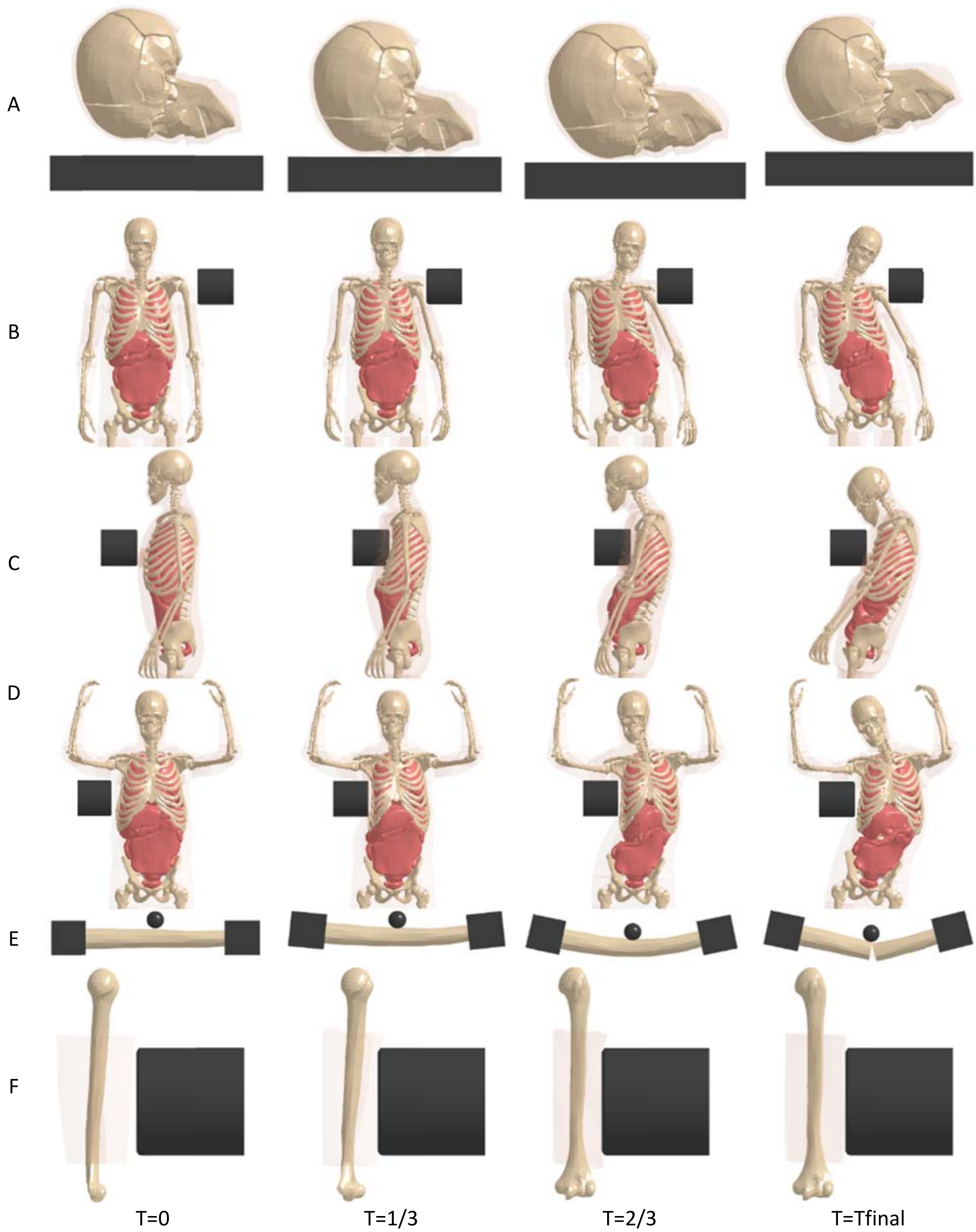

Fig. 2. Simulation time-lapse for (a) head drop impact, (b) shoulder impact, (c) thoracic frontal impact, (d) thoracic lateral impact, (e) humerus three-point bending, (f) arm compression. The model response shown is the baseline pedestrian model (AM50-P) response.

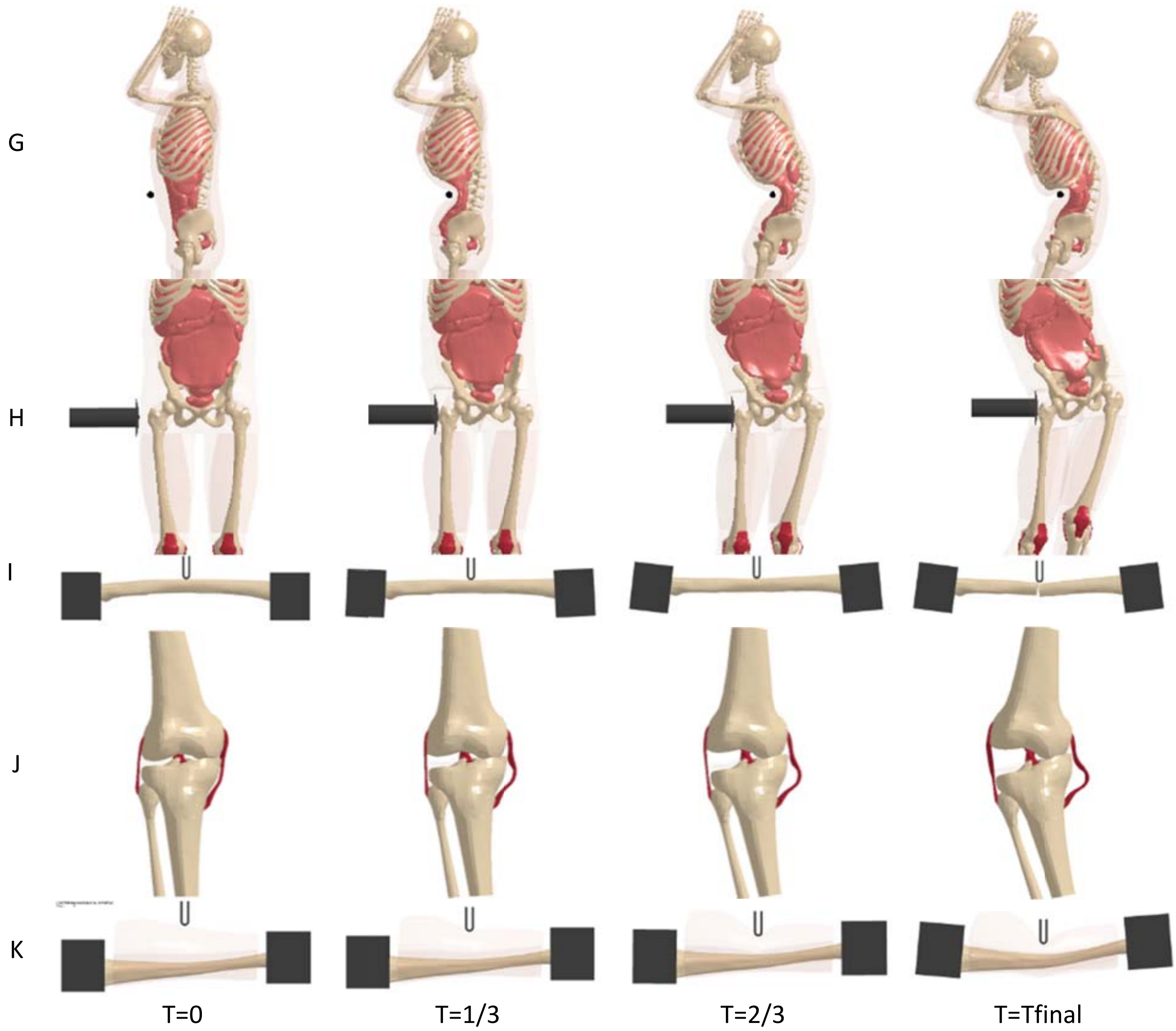

Fig. 2. (*continued*) Simulation time-lapse for (g) abdominal impact, (h) pelvic impact, (i) femur three-point bending, (j) knee three-point bending, (k) leg three-point bending. The model response shown is the baseline pedestrian model (AM50-P) response.

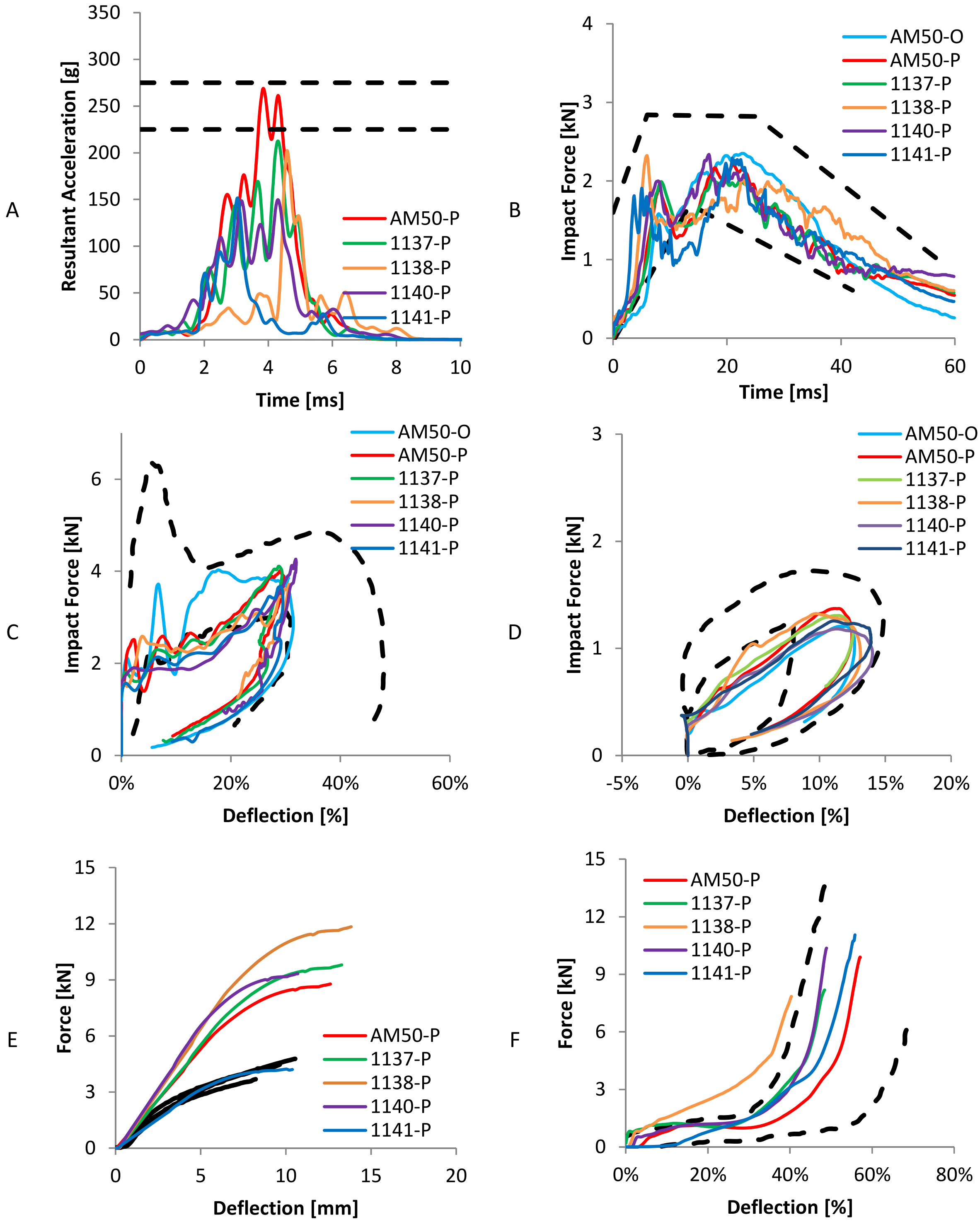

Fig. 3. Model responses (AM50-O: light blue, AM50-P: red, 1137-P: green, 1138-P: orange, 1140-P: purple, 1141-P: dark blue) compared to experimental corridors/requirements (black) for (a) head drop impact, (b) shoulder impact, (c) thoracic frontal impact, (d) thoracic lateral impact, (e) humerus three-point bending, (f) arm compression.

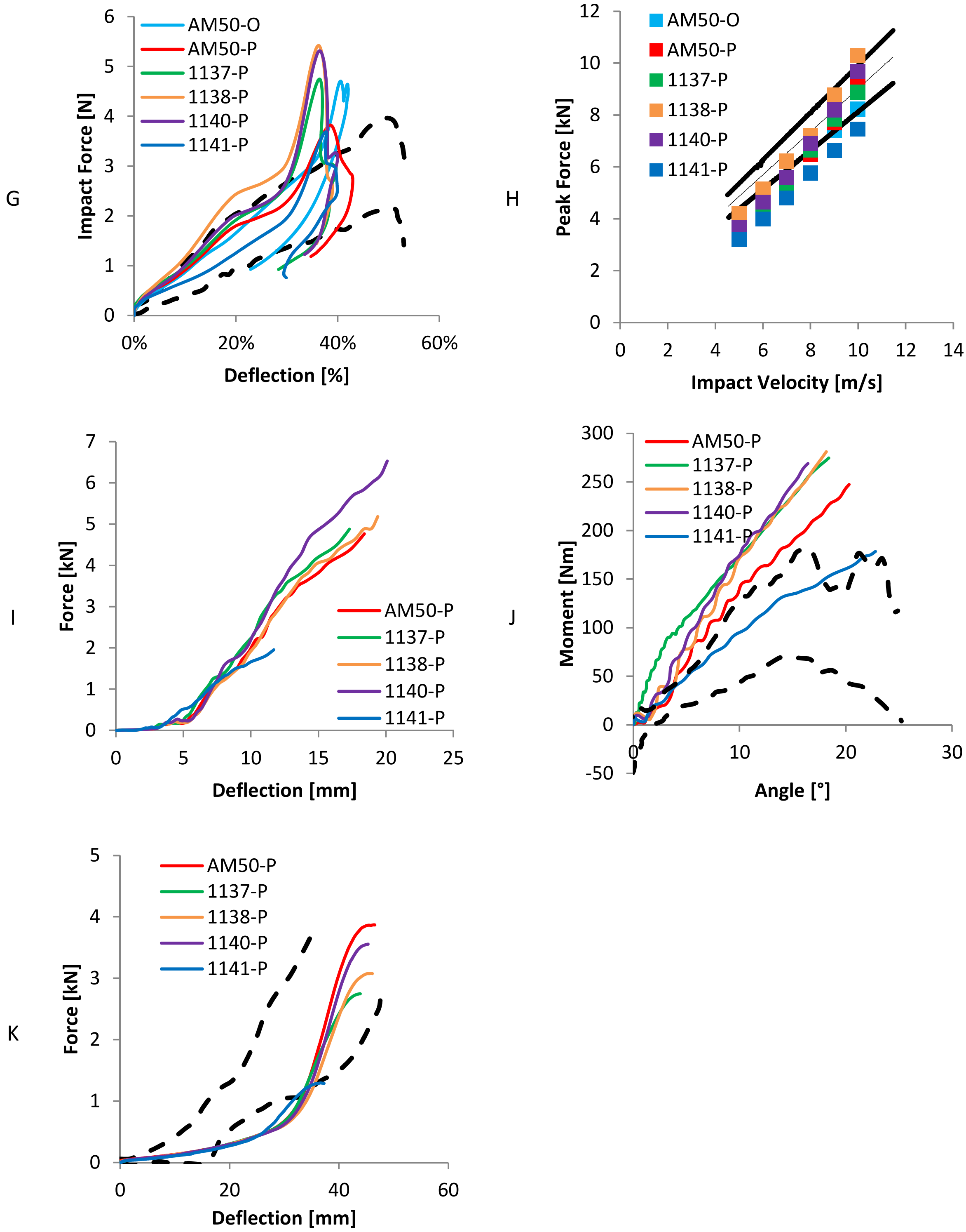

Fig. 3. (*continued*) Model responses (AM50-O: light blue, AM50-P: red, 1137-P: green, 1138-P: orange, 1140-P: purple, 1141-P: dark blue) compared to experimental corridors/requirements (black) for (g) abdominal impact, (h) pelvic impact, (i) femur three-point bending, (j) knee three-point bending, (k) leg three-point bending.

VIII. APPENDIX

TABLE A

EXTERNAL ANTHROPOMETRIC MEASUREMENTS USED FOR MORPHING

ID	Anthropometric measurements		AM50-P	1137-P / *PMHS 1137*	1138-P / *PMHS 1138*	1140-P / *PMHS 1140*	1141-P / *PMHS 1141*
1	*Stature [mm]*		1771	1597 / *1540*	1903 / 1870	1666 / 1610	1839 / 1820
2	*Weight [kg]*		77	66 / 73	119 / 114	84 / 86	55 / 46
3	*Top of Head- to- Trochanterion*		880	808 / 785	914 / 890	803 / 790	837 / 860
4	*Shoulder (Acromial) Height*		1522	1365 / 1330	1675 / 1630	1410 / 1380	1593 / 1570
5	*Waist Depth - Umbilicus*		234	215 / 200	360 / 360	313 / 300	163 / 140
6	*Waist Breadth*		343	358 / 370	425 / 440	379 / 390	298 / 290
7	*Shoulder Breadth (Biacromial)*		354	364 / 370	390 / 370	349 / 350	325 / 330
8	*Chest Breadth*	*4th rib*	314	345 / 360	406 / 420	336 / 340	266 / 265
9		*8th rib*	335	347 / 340	416 / 410	374 / 380	282 / 270
10	*Chest Depth*	*4th rib*	239	210 / 220	316 / 320	248 / 250	203 / 210
11		*8th rib*	246	229 / 230	356 / 350	303 / 290	209 / 220
12	*Hip Breadth*		353	363 / 360	419 / 410	405 / 400	303 / 310
13	*Buttock Depth*		208	202 / 205	302 / 300	233 / 230	193 / 200
14	*Shoulder- to- Elbow*		329	343 / 350	420 / 430	340 / 345	397 / 410
15	*Forearm- to- Hand*		395	401 / 420	424 / 450	396 / 400	418 / 450
16	*Tibial Height*		460	419 / 425	453 / 450	398 / 400	505 / 515
17	*Ankle Height (outside)*		80	77 / 80	94 / 120	76 / 120	97 / 110
18	*Foot Breadth*		90	109 / 80	109 / 100	104 / 100	90 / 90
19	*Foot Length*		270	227 / 210	281 / 250	241 / 240	255 / 260
20	*Head Length*		190	190 / 180	210 / 210	190 / 190	199 / 200
21	*Head Breadth*		150	189 / 160	189 / 190	160 / 160	150 / 150
22	*Head Height*		239	225 / 200	222 / 220	230 / 230	221 / 220
23	*Neck Circumference*		370	417 / 424	439 / 440	473 / 490	353 / 350
24	*Thigh Circumference*		515	502 / 520	625 / 630	580 / 580	403 / 380
25	*Lower Thigh Circumference*		360	329 / 350	393 / 450	389 / 410	321 / 300
26	*Knee Circumference*		361	320 / 350	382 / 390	381 / 390	316 / 330
27	*Calf Circumference*		359	341 / 335	381 / 380	375 / 375	222 / 220
28	*Ankle Circumference*		251	228 / 205	253 / 225	254 / 230	202 / 180
29	*Bicep Circumference*		309	314 / 310	362 / 365	306 / 310	253 / 165
30	*Elbow Circumference*		275	295 / 290	325 / 320	254 / 250	219 / 210
31	*Forearm Circumference*		261	269 / 265	317 / 320	252 / 255	198 / 190
32	*Wrist Circumference*		156	154 / 160	175 / 175	153 / 160	146 / 155

A

B

C

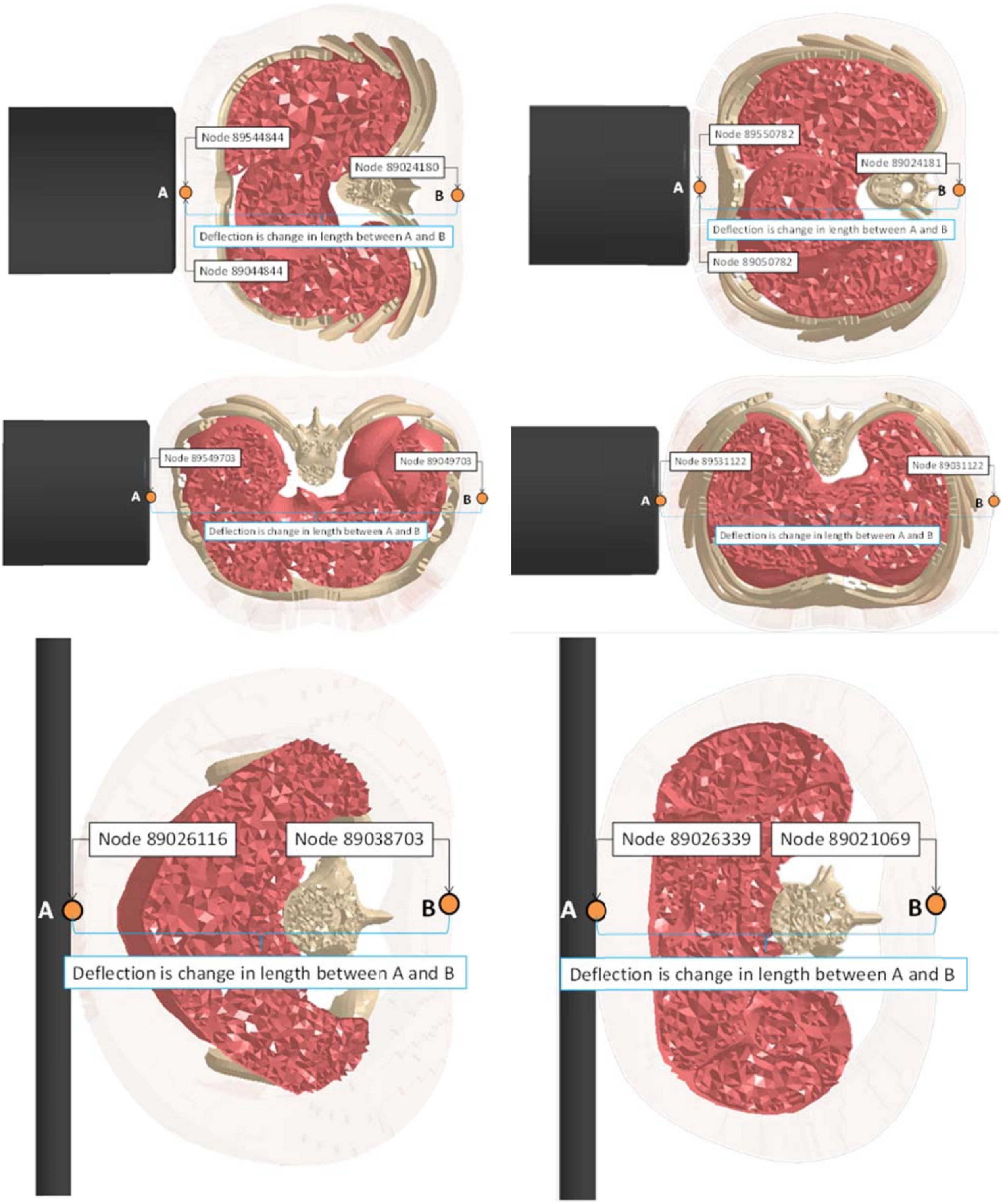

AM50-O AM50-P

Fig. A. Superior view of the cross-section of the thorax at different levels, showing the points used to measure the deflection in the occupant model (AM50-O) and the pedestrian model (AM50-P) for (a) thoracic frontal impact, (b) thoracic lateral impact, (c) abdominal impact.